Comparison of the open-closed separatrix in a global magnetospheric simulation with observations: the role of the ring current

Comparison of the open-closed separatrix in a global magnetospheric simulation with observations: The role of the ring current

I. J. Rae,[1] K. Kabin,[1] J. Y. Lu,[2] R. Rankin,[1] S. E. Milan,[3] F. R. Fenrich,[1] C. E. J. Watt,[1] J.-C. Zhang,[4] A. J. Ridley,[5] T. I. Gombosi,[5] C. R. Clauer,[6] G. Tóth,[5] and D. L. DeZeeuw[5]

Received 2 November 2009; revised 4 March 2010; accepted 12 March 2010; published 17 August 2010.

[1] The development of global magnetospheric models, such as Space Weather Modeling Framework (SWMF), which can accurately reproduce and track space weather processes has high practical utility. We present an interval on 5 June 1998, where the location of the polar cap boundary, or open-closed field line boundary (OCB), can be determined in the ionosphere using a combination of instruments during a period encompassing a sharp northward to southward interplanetary field turning. We present both point- and time-varying comparisons of the observed and simulated boundaries in the ionosphere and find that when using solely the coupled ideal magnetohydrodynamic magnetosphere-ionosphere model, the rate of change of the OCB to a southward turning of the interplanetary field is significantly faster than that computed from the observational data. However, when the inner magnetospheric module is incorporated, the modeling framework both qualitatively, and often quantitatively, reproduces many elements of the studied interval prior to an observed substorm onset. This result demonstrates that the physics of the inner magnetosphere is critical in shaping the boundary between open and closed field lines during periods of southward interplanetary magnetic field (IMF) and provides significant insight into the 3-D time-dependent behavior of the Earth's magnetosphere in response to a northward-southward IMF turning. We assert that during periods that do not include the tens of minutes surrounding substorm expansion phase onset, the coupled SWMF model may provide a valuable and reliable tool for estimating both the OCB and magnetic field topology over a wide range of latitudes and local times.

Citation: Rae, I. J., et al. (2010), Comparison of the open-closed separatrix in a global magnetospheric simulation with observations: The role of the ring current, *J. Geophys. Res., 115,* A08216, doi:10.1029/2009JA015068.

1. Introduction

[2] Global magnetospheric models [*Ogino*, 1986; *Raeder et al.*, 1995; *White et al.*, 1998; *Fedder and Lyon*, 1995, 1997; *Winglee et al.*, 1998; *Gombosi et al.*, 2000] are becoming increasingly invaluable tools for field line mapping [e.g., *Elsen et al.*, 1998; *Raeder et al.*, 1998; *Garcia and Hughes*, 2007]. However, the global results obtained from large-scale magnetohydrodynamic (MHD) models are difficult to validate routinely, due to the rarity of true global coverage of observational data. A partial validation of global MHD results has been achieved with point-to-point comparisons, for example, between modeled magnetic fields and those measured by satellites [e.g., *Fedder et al.*, 1997]. Previous validation studies of global circulation models have also used the location of the boundary between closed magnetic flux and flux interconnected with the solar wind, that is, the open-closed field line boundary (OCB) [e.g., *Elsen et al.*, 1998; *Raeder et al.*, 1998 and 2000; *Rae et al.*, 2004]. This boundary is important for several reasons. First, it is one of the most important topological interfaces in the magnetosphere and knowing its location is crucial for understanding and interpretation of plasma convection processes [e.g., *Watanabe et al.*, 2005; *Hubert et al.*, 2006]. It is also closely associated with the amount of magnetic energy stored in the magnetosphere and is, therefore, essential for analysis of storm and substorm dynamics. When the interplanetary magnetic field (IMF) has a southward component, reconnection may take place between the IMF and the

[1]Department of Physics, University of Alberta, Edmonton, Alberta, Canada.
[2]National Center for Space Weather, China Meteorology Administration, Beijing, China.
[3]Department of Physics and Astronomy, University of Leicester, Leicester, UK.
[4]Space Science Center, University of New Hampshire, Durham, New Hampshire, USA.
[5]Center for Space Environment Modeling, University of Michigan, Ann Arbor, Michigan, USA.
[6]Department of Electrical and Computer Engineering, Virginia Polytechnic Institute and State University, Blacksburg, Virginia, USA.

0148-0227/10/2009JA015068

closed terrestrial field on the dayside magnetopause, opening new flux and increasing the polar cap area, which is bounded in the ionosphere by the OCB. Conversely, when nightside reconnection processes occur, open flux is destroyed, decreasing the polar cap area. The balance between the two will thus be reflected in the rate of change of polar cap area [e.g., *Cowley and Lockwood*, 1992; *Milan et al.*, 2007].

[3] *Rae et al.* [2004] compared point measurements of the OCB as determined by the Canadian Auroral Network for the OPEN Program Unified Study [*Rostoker et al.*, 1995] Meridian Scanning Photometers with the steady state block adaptive-tree solar wind roe-type upwind scheme (BATS-R-US) MHD code [*Powell et al.*, 1999]. This study was conducted to estimate the accuracy of the OCB calculated by this model as compared to point observations at a single ground station as a function of magnetic local time (MLT). *Rae et al.* [2004] concluded that the estimate of the OCB obtained from the model was on average an excellent indicator of the location and motion of the poleward boundary of the red line auroral emission over a range of MLTs in the premidnight and postmidnight sectors (~2100–0100 MLT) during steady magnetospheric convection [*Yahnin et al.*, 1994] intervals. In a companion study, *Kabin et al.* [2004] used the same BATS-R-US MHD code as that of *Rae et al.* [2004] to study the OCB dependence on the solar wind and IMF parameters but did not directly compare their modeled results with measurements.

[4] *Elsen et al.* [1998] compared the results of the Winglee MHD model [*Winglee et al.*, 1998] with the poleward boundary of Polar Ultraviolet Imager (UVI) emissions for a period of ~3.5 h and found that there was a reasonable reproduction of the observed OCB (~2°) at 1200 MLT for some parts of the time interval, but this discrepancy increased to 3°–10° on the flanks and to ~20° at local midnight at times.

[5] *Raeder et al.* [1998] used the global geospace circulation model (GGCM) to compare low-altitude spacecraft observations of precipitation boundaries with simulation results and found that the simulations generally agreed well with observed in situ particle precipitation boundaries, with the exception of the dusk sector, where there was a region of soft electron precipitation that lay significantly poleward of the simulation results. The latter was attributed to either polar cap precipitation or a breakdown of the assumptions inherent in their model. *Raeder et al.* [2000] subsequently used the GGCM to model an observed substorm and found that although polar cap open fluxes could be compared well with Polar visible light spectrometer estimates, the auroral currents associated with substorm onset could not be modeled realistically. In their study, *Raeder et al.* [2000] found that for a large range of model parameters, a substorm could not be triggered, steady magnetospheric convection dominated the simulation, and no explosive reconfiguration of the magnetosphere, such as a substorm could be triggered. The authors concluded that their simulations would benefit from three model improvements: improved auroral conductance, anomalous resistivity, and better treatment of the ring current.

[6] A more comprehensive method to assess the global accuracy of a magnetospheric model is via monitoring a full 2-D OCB. Unfortunately, current observations provide such global data sets only very infrequently; however, *Milan et al.* [2003] used a multi-instrument observational technique to provide estimates of the 2-D location and dynamics of the OCB during a ~7 h period encompassing two substorm cycles. In their paper, *Milan et al.* [2003] used measurements from the Super Dual Auroral Radar Network (SuperDARN) HF radar network [*Greenwald et al.*, 1995], the Polar UVI [*Torr et al.*, 1995], and particle detectors onboard a suite of low-earth orbit spacecraft to determine the location of the OCB over as wide an MLT extent as possible over a 7 h interval (see *Milan et al.* [2003] for details). Although recently, there have been a number of studies which attempt to quantify the accuracy of the output of MHD-based models using both point observations and empirical-based models the present study using unique fully 2-D observations of the OCB represents an exceptional opportunity to assess the validity and accuracy of global models such as the Space Weather Modeling Framework (SWMF) [*Toth et al.*, 2005]. In this paper we use a subset of the interval studied by *Milan et al.* [2003] during which a sharp northward to southward IMF transition was observed, to provide a ~2 h period of comparison of the global MHD runs with the determination of the OCB outlined in the study of *Milan et al.* [2003].

[7] Previous OCB modeling attempts mostly utilized magnetospheric models based on ideal MHD [e.g., *Elsen et al.*, 1998; *Raeder et al.*, 1998, 2000; *Rae et al.*, 2004; *Kabin et al.*, 2004] and therefore were unable to address the effects of the inner magnetosphere and, in particular, of the ring current on the OCB location. However, in addition to the IMF orientation, dayside reconnection can be affected by a number of processes in the inner magnetosphere. For example, *Su et al.* [2000] and *McFadden et al.* [2008] presented clear evidence that cold dense plasmaspheric plasma may play an important role in dayside reconnection. The plasma pressure supplied by the inner magnetosphere significantly affects plasma drift and is required to produce realistic magnetopause standoff distances. While the inclusion of a plasmasphere does not directly affect the magnetospheric magnetic field configuration, the cold plasma still contains most of the mass of the magnetosphere and is significant for the reconfiguration dynamics. The ring current carries a large percentage of the total particle energy and sufficient current to directly affect the magnetic field configuration (see review by *Toffoletto et al.* [2003]). In this paper we use a recently developed global circulation mode that includes fully coupled MHD and kinetic inner magnetosphere modules [*Toth et al.*, 2005], thus, allowing us to investigate some of those important effects for the first time.

[8] This paper provides a summary of the observational data presented in the study of *Milan et al.* [2003] and compares the OCB obtained observationally with the computed OCB from two of the configurations of the coupled models within the Space Weather Modeling Framework (SWMF). One of the considered model configurations did not include the coupled inner magnetosphere model, while the other did. Although the results are variable in the nightside magnetosphere, we conclude that the model configuration without the inner magnetospheric module provides a reasonable reproduction of the polar cap boundary for ~1 h after a southward turning of the IMF and then begins to underestimate the amount of open flux in the Earth's magnetosphere. When the inner magnetospheric

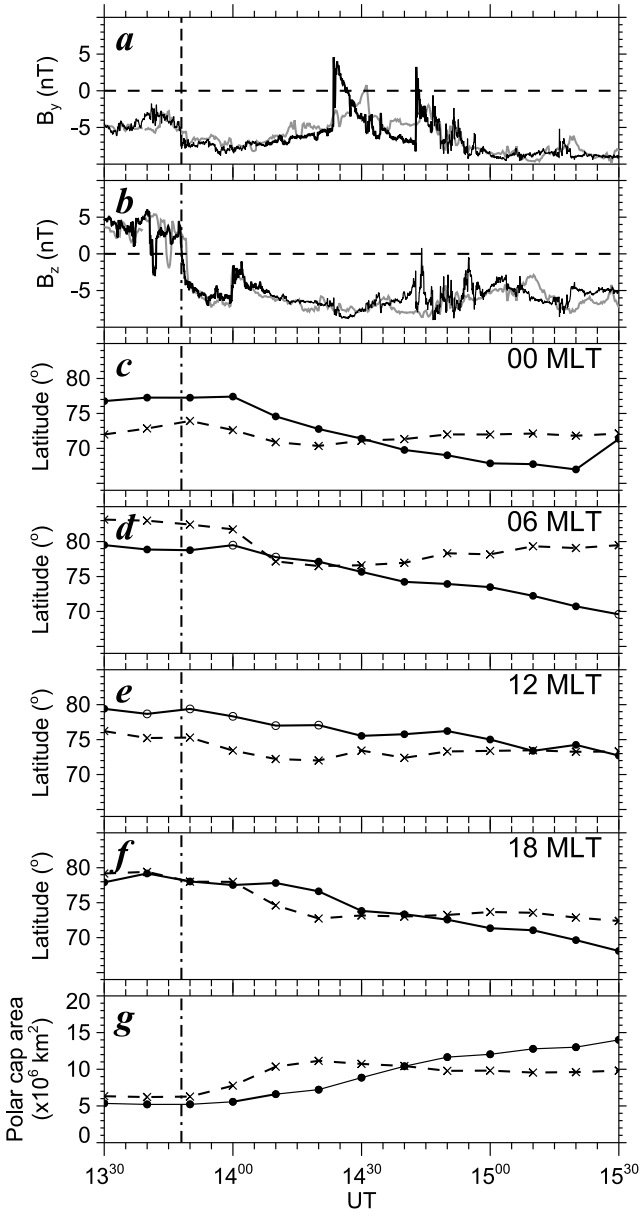

Figure 1. An overview of 5 June 1998 event presented by *Milan et al.* [2003]. Time series of (a) IMF B_y and (b) IMF B_z measured by the Wind (black line) and ACE (gray line) on the 5 June 1998 0900–1630 UT, suitably lagged to the magnetopause. Also included in Figure 1 are time series of OCB latitudes of the observed (solid line and circles) and BATS-R-US-IE modeled (dashed and crosses) data along the (c) midnight, (d) dawn, (e) noon, and (f) dusk meridians. For the observational time series, filled circles represent data points that are determined by actual observational measurements. If there is no nearby auroral measurement, the OCB is interpolated from the earlier and later MLTs and shown by the open circles. Figure 1g shows the variations in modeled and observed polar cap area during this interval (see text for details). Vertical lines in all panels denote the northward to southward transition of the IMF.

model is included, the observed and modeled OCBs are in much better qualitative agreement for a large range of both UT and local times. We discuss the limitations and potential applications of these results and demonstrate that the inner magnetosphere contributes heavily to the location of the open-closed field line boundary.

2. The Space Weather Modeling Framework (SWMF)

[9] The SWMF is a recently developed suite of computational models that can be used for modeling physical processes from the Sun to the Earth [e.g., *De Zeeuw et al.*, 2004; *Toth et al.*, 2005]. The SWMF consists of several numerical modules, such as the ideal MHD solver (BATS-R-US) [*Powell et al.*, 1999], ionospheric electrodynamics (IE) model [*Ridley et al.*, 2002], and Rice Convection Model (RCM) [*Toffoletto et al.*, 2003]. In this paper we compare results of two configurations of the SWMF: incorporating the BATS-R-US and IE coupled model, and the BATS-R-US, IE, and RCM coupled model. The first of these configurations has been used extensively to study various solar wind influences on the magnetosphere, for example, northward IMF [*Song et al.*, 1999; *Watanabe et al.*, 2005], IMF by effects [e.g., *Kabin et al.*, 2003], and Parker spiral angles [*Gombosi et al.*, 2000]. The more recent SWMF configuration including a fully coupled RCM module has been used, for example, for southward IMF [*De Zeeuw et al.*, 2004] and for studying storm dynamics [*Zhang et al.*, 2007; *Toth et al.*, 2007].

3. Data and Model Comparisons

3.1. Description of the Event

[10] Figures 1a and 1b show the IMF B_y and B_z conditions, respectively, between 1330 and 1530 UT on 5 June 1998 from both the Wind (black line) and ACE (gray line) spacecraft. These measurements are suitably lagged to the magnetopause with delays of 66 and 78 min, respectively (see *Milan et al.* [2003] for details). This interval encompasses a sharp southward turning in the IMF, which is both preceded and followed by a period of relatively steady IMF conditions. During this interval, B_y was approximately −5 nT (apart from two excursions around 1425 UT and 1445 UT), while B_z undergoes a sharp transition from a northward (+5 nT) to southward (−5 nT) orientation just prior to 1350 UT. It is this transition that we focus on in this paper. Both configurations of the SWMF were run to quasi steady state conditions using the Wind IMF data at 1330 UT. This time was chosen as it corresponds to the end of a period of relatively steady (and northward) IMF conditions, which we assume allows a steady state solution to approximate the state of the magnetosphere. From the resulting steady state solution, each model configuration was run in time-varying mode for the 2 h period 1330–1530 UT. It should be noted that the initialization of global circulation models remains a difficult problem, which is unlikely to be completely resolved until the density of measurements in the terrestrial magnetosphere increases significantly. While the procedure described above is certainly reasonable, there is no guarantee that the modeled magnetosphere accurately represents the actual magnetosphere at the very beginning of the sim-

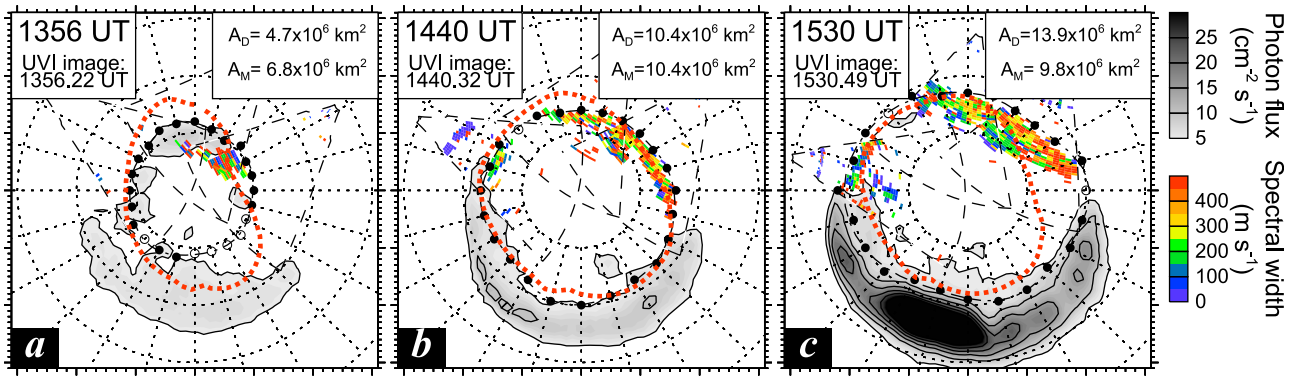

Figure 2. Three composite plots of Polar UVI auroral intensity (gray scale) and SuperDARN HF radar spectral widths (color scale) in magnetic latitude (MLAT): magnetic local time (MLT) coordinates. Dotted circles represent 60°, 70°, and 80° MLAT, and radial lines represent MLT meridians, with noon at the top of the page. Overplotted upon this is the observed (dash-dotted line and circles) and BATS-R-US-IE (red dashed line). In each frame, Polar UVI data are shown as gray scale and SuperDARN spectral widths as color. The OCB was determined experimentally by taking the poleward edge of high-energy (1–10 keV) electron precipitation [e.g., *Evans and Stone*, 1972], while the equatorward edge of the ~250 m/s SuperDARN spectral widths and the poleward gradient in Polar UVI emissions are employed as proxies for the OCB on the dayside and nightside, respectively. For brevity, particle precipitation boundaries that were also used to determine the observed OCB are not shown [see *Milan et al.*, 2003 for details] but are included in the observational estimate of the OCB. The red dashed line represents the OCB as determined by the model. Filled circles represent MLT sectors that an OCB measurement could be derived observationally, while if there were no nearby measurement, the OCB is interpolated from the earlier and later MLTs and shown by open circles. Figure 2a shows the comparison at 1356 UT, under northward IMF conditions. Figure 2b shows the comparison at 1440 UT, some time after the southward IMF turning and Figure 2c shows the comparison at the end of the simulated interval at 1530 UT. In the top right hand corner of each plot is the observed (A_D) and modeled (A_M) polar cap areas derived by numerically integrating the size of each MLT sector (for details see text).

ulation. Each simulation involved ~4 × 10^6 computational cells with the smallest cell size equal to 0.25 R_E.

3.2. BATS-R-US and IE-Only Comparison

[11] Figures 1c, 1d, 1e, and 1f show latitude time plots of both the observed and modeled OCB as determined along the midnight, dawn, noon, and dusk meridians, respectively. The circles and solid line represent the observational data as shown in the study of *Milan et al.* [2003], whereas the crosses and dashed line represent the model results. From these plots we are able to provide a quantitative comparison between the observed and modeled polar cap boundary. There are several points to note from Figures 1c to 1f. First, the differences between observed and modeled results have a strong MLT dependence. The OCB remains relatively constant between 71° and 74° at midnight in the model, whereas the observational boundary varies from an initial location of 77°–67° at the end of the interval, crossing the model boundary at 1430 UT. At noon, the model OCB is 3° equatorward of the observed boundary at the start of the interval (under northward IMF), but both converge to the same latitude (73°) at the end of the interval. From Figures 1d and 1f, respectively, it can be seen that the comparison at dusk is better than at dawn. Around dawn, the model OCB is several degrees poleward of the observed boundary at the start of the interval but proceeds to progress equatorward to the same latitudes as the observed boundary between 1410 and 1430 UT. However, the dawnside model boundary proceeds to contract poleward thereafter and concludes the interval at 80°, some 10° poleward of the observed boundary. This situation is not mirrored at dusk, where the model and observed boundaries both begin the interval at ~80°. The model boundary there responds first to the southward turning and proceeds to lower latitudes at 1400 UT, whereas the observed boundary does not begin to move to lower latitudes until 1410 UT. The model boundary then remains at ~73° for the remainder of the interval while the observed OCB continues to evolve to lower latitudes, ending the interval at ~68°.

[12] Figure 1g shows the comparison between polar cap areas for the observational data (A_D) and the model (A_M), derived by numerically integrating the size of each MLT sector. From Figure 1g, we can see that the observed and modeled polar caps are similar and relatively constant until ~1350 UT, where the model underwent a rapid expansion in polar cap area for around 30 min from ~7 to 10.5 × 10^6 km^2 and remains relatively constant for the remainder of the interval. This is in contrast to the observational polar cap area, which starts to respond to the southward turning of the IMF at ~1400 UT and grows in area from ~5 to 14 × 10^6 km^2 between 1400 and 1520 UT. From this initial configuration, it can be seen that the initial rate of increase of polar cap area is greater in the model than the observations.

[13] Figure 2 shows the comparison between the BATS-R-US-IE model and the observed OCB in magnetic latitude-magnetic local time (MLAT-MLT) coordinates (with noon at the top of the plot) for 3 times during the interval, immediately following the southward IMF turning (1356 UT), the

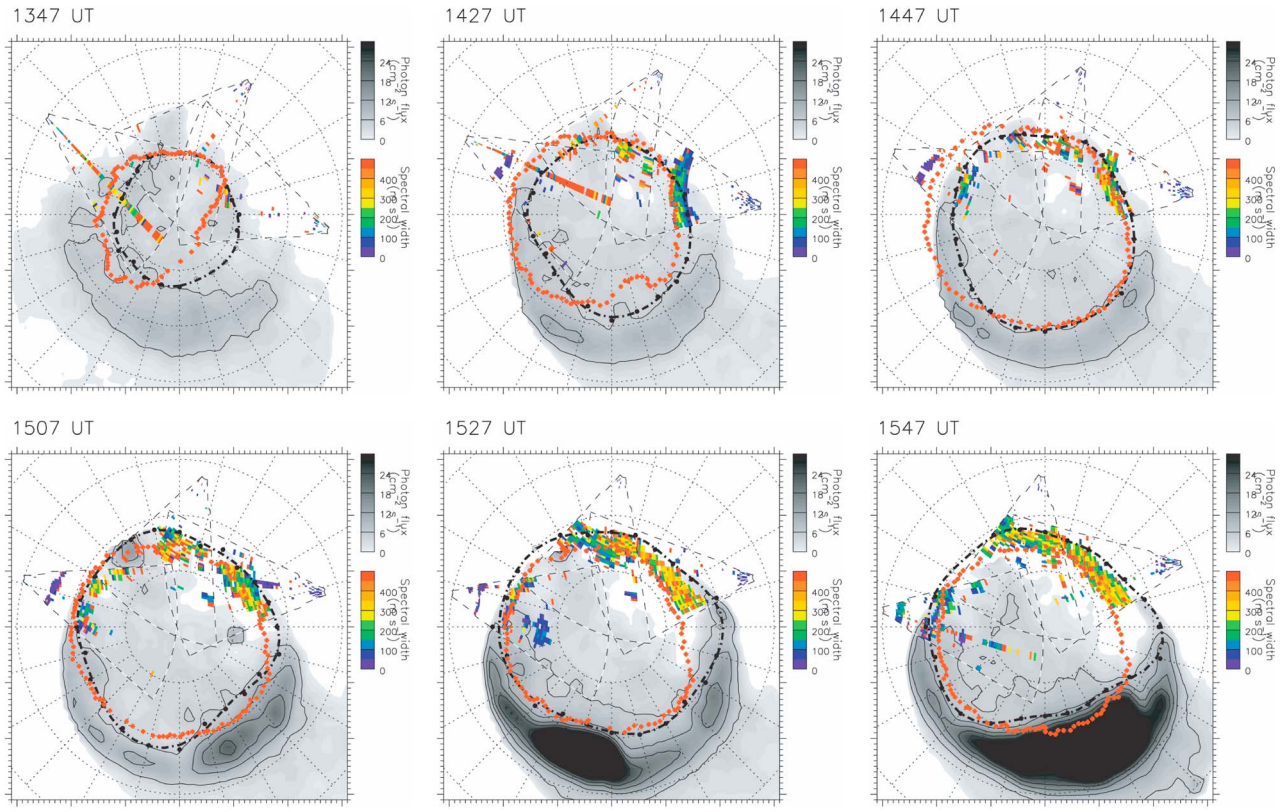

Figure 3. Comparison of the observed and BATS-R-US-IE-RCM OCBs for the same interval, in the same format as Figure 2 for 6 times during the northward to southward IMF transition.

time of best comparison (1440 UT), and the end of the simulated interval (1530 UT). Figures 2a–2c show a Polar UV image (gray scale), and backscatter was observed simultaneously from three of the six SuperDARN HF radars for clarity (in color). Figures 2a–2c also show the model (red line) and observation-derived (black circles) OCBs (see Figure 2 caption for details). Finally in the top right hand corner of each plot is an estimate of the polar cap area for the observational data (A_D) and the model (A_M) for comparison.

[14] We can see from Figure 2a that the BATS-R-US-IE model OCB immediately subsequent to the southward turning is not consistent with the observational OCB, other than around the dusk flank. Indeed, in the noon-midnight meridian, the model OCB is up to 7° equatorward of the observed boundary. Furthermore, around dawn, the model boundary exhibits a concave configuration, and is actually poleward of the observed boundary. The inaccuracies in the model boundary configuration are reflected in the near 50% overestimation of the polar cap area as determined by the observations. Figure 2b, however, is more encouraging; at 1440 UT, there is good correlation between the two boundaries on a near-global scale. The observed and modeled boundaries appear to be almost entirely consistent with one another, other than a section between 12 and 14 MLT, and even in this MLT sector, the difference between model and observations is only 3°. Furthermore, the polar cap areas are identical, both ~10.4×10^6 km^2. However, this situation does not last, as shown in Figure 1, and at 1530 UT, the BATS-R-US-IE polar cap has shrunk from its previous configuration, while the observed polar cap is still growing due to the continued opening of flux on the dayside (Figure 2c). The comparison between these boundaries is still reasonable for ~1200–1700 MLT and ~2200–0100 MLT; however, at dawn and dusk, the differences are marked. Around dusk, the modeled boundary is ~5° poleward of the observed boundary, and at dawn, it appears to be returning to its initial concave configuration where it is ~10° poleward of the observed boundary.

3.3. BATS-R-US, IE, and RCM Model Comparison

[15] One of the primary reasons for the poor reproduction of observed features in MHD modeling may be the topology of the magnetotail obtained using just the BATS-R-US-IE coupled model. This problem is at least partly addressed by the addition of the RCM [*De Zeeuw et al.*, 2004, their Figure 4], whereby the improved modeling of the physics of the inner magnetosphere typically results in a doubling of the inner magnetospheric pressure that pushes the reconnection X line much further into the magnetotail to $X = -26$ to 34 R_E (compare, 8–10 R_E in the model configuration outlined in section 3.2). The resulting magnetospheric configuration is expected to provide a much more realistic magnetic topology in a moderately stretched magnetospheric state and so should be able to reproduce the large-scale configuration of the magnetosphere more readily.

[16] Figure 3 shows 6 snapshots of the 2-D observed and modeled OCB in the same format as Figure 2. Figure 3

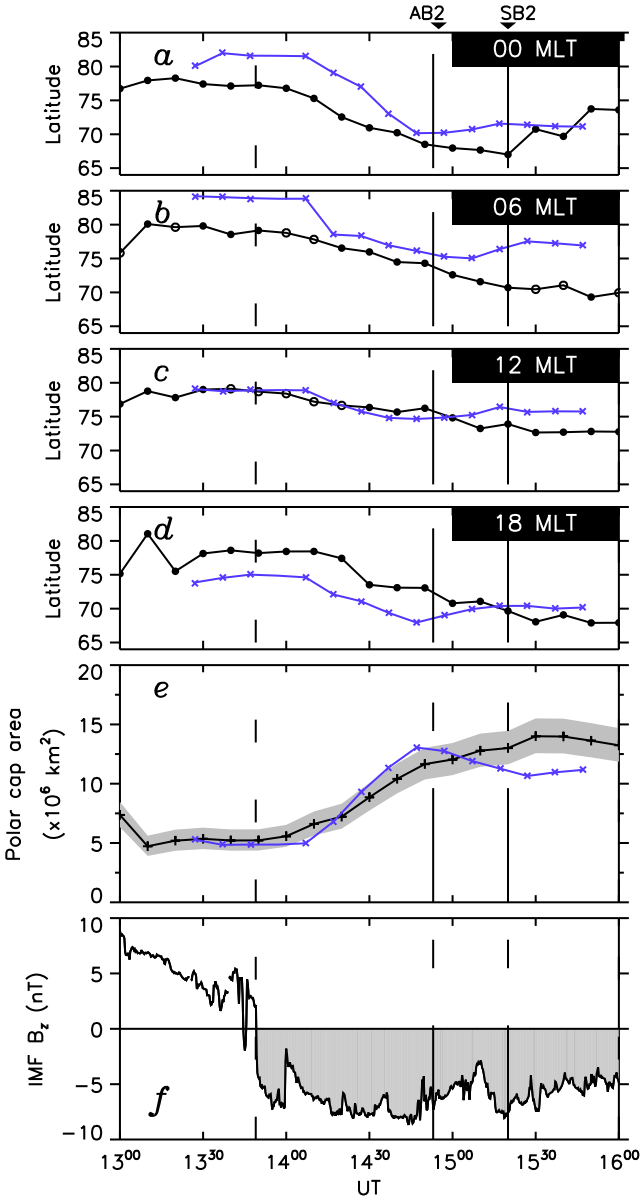

Figure 4. Time series comparison of the observed (circles and solid line) and BATS-R-US-IE-RCM modeled (crosses and solid line) OCBs for (a) midnight, (b) dawn, (c) noon, and (d) dusk meridians. (e) Variations in modeled and observed polar cap area during this interval, together with an estimated error range, obtained by assuming a ±1° error at all MLTs. (f) The IMF B_z component for reference. From left to right, the vertical lines in all frames denote the northward to southward transition of the IMF, the auroral brightening (AB2) and the substorm expansion phase onset (SB2).

denotes the model and observed boundaries during the simulation interval, from close to the start of the simulation interval at 1347 UT, and then at 20 min intervals from 1427 to 1547 UT. What is immediately obvious in Figure 3 is the excellent colocation of the observed and modeled OCBs at a number of local times as the interval progresses. At 1347 UT, there is a perfect comparison on the dayside in the 0800–1400 MLT range, but this result is offset by the poor comparison in the postmidnight to dawn sector. However, as the north-south solar wind B_z transition begins to fully affect the magnetosphere after ~1400 UT, the OCB estimates become much more similar. At 1427 UT, the observed OCB in the ~0200–1300 MLT sector is very well described in the model, being separated by a maximum of ~3° of latitude over this region. Indeed, the 0800–1300 MLT region is perfectly described by the model OCB. The modeled OCB in the postnoon to premidnight sector, however, is ~4° equatorward of the observed OCB. As the southward IMF continues to inflate the polar cap, the comparison between the observed and modeled OCB is remarkably good on a near-global scale. At 1447 UT, the observed and modeled OCBs lie within 1° of each other over a large range of MLT (2200–1300 MLT covering the dawn side of the polar cap), though the comparison is not accurate in the dusk to premidnight sector and differs by 4°–5°. The comparison improved even further by 1507 UT, when there is an excellent correspondence between the observed and modeled OCBs, with the largest discrepancies of ~3° at 0200–0300 MLT (again, close to an auroral intensification). Although the substorm onset (at ~1520 UT) drastically reconfigures the magnetospheric topology, the comparison at 1527 and 1547 UT remains remarkably accurate for most local time sectors. The 0400–1000 MLT sector contains the largest discrepancy between the observed and modeled OCBs, the model OCB being situated up to 7° poleward of the observations. We discuss the potential reasons for this discrepancy in section 4.

[17] To further demonstrate the details of the OCB evolution, in Figure 4, we isolate four local times and follow the progress of the boundary location in the same manner as Figure 1. We also plot IMF B_z component for context (Figure 4f). The modeled OCB at midnight (Figure 4a) is significantly poleward of the observed OCB during the northward IMF section of the interval, but as the IMF turns southward, the OCB progresses to lower latitudes and starts to reproduce the observed OCB well prior to the substorm expansion phase onset around 1520 UT. At dawn (Figure 4b), the model OCB is at higher latitudes than the observed OCB; after the southward turning and a reasonable colocation of the observed and modeled boundaries, the modeled OCB returns to higher latitudes significantly quicker than the observed OCB and after 1500 UT. At noon (Figure 4c), the observed and modeled OCBs are similar for the majority of the interval, before the modeled OCB progresses to higher latitudes than the observed OCB around 1500 UT. At dusk (Figure 4d), the modeled OCB is at significantly lower latitudes than the observed OCB prior to the auroral brightening but does mimic the behavior of the dusk sector boundary motion well. Subsequent to the auroral brightening, the dusk sector comparisons improve significantly, and the observed and modeled OCBs are reasonably well colocated. The improved OCB boundary location modeled by the BATS-R-US-IE-RCM model is reflected in the excellent comparison (within experimental errors) between the observed and modeled polar cap areas (Figure 4e) at all times up until ~1520 UT. Following this period, from 1520 UT until the end of the interval, the modeled OCB significantly underestimates the size of the polar cap, which coincides

with the time of auroral substorm onset, presumably corresponding to the initiation of the closure of a significant amount of open flux in the magnetosphere.

4. Discussion

[18] The ability to monitor the polar cap area allows the investigation of the amount of closed magnetic flux and flux interconnected with the solar wind and, therefore, the storage and release of magnetic energy during the substorm cycle. In practice, however, it is very difficult to identify the OCB location unambiguously. In fact, it is usually necessary to use proxies for the OCB from many different data sets, where particle precipitation boundaries are considered to be the clearest indication of an open-closed field line transition. Previous comparisons of particle precipitation and poleward spacecraft UV boundaries have determined that there may be discrepancies on the order of degrees [e.g., *Kauristie et al.*, 1999] between the precipitation boundary and UV proxy. Furthermore, *Baker et al.* [2000], *Carbary et al.* [2003], and *Wild et al.* [2004] indicated that the largest inconsistency between precipitation and other OCB proxies is in the dawn sector. *Wild et al.* [2004] suggested that the most reliable way to determine the dawnside OCB was to utilize two discrete wavelengths of UV emissions and compare the results to precipitation boundaries where available; this suggestion was recently verified by *Boakes et al.* [2009]. The typical differences between the two auroral boundaries are on average about 2°, which may be partially responsible for some of the dawn sector discrepancies shown in Figure 3. Since the least favorable comparison between the observed and modeled OCBs consistently occur in the dawn sector during the southward IMF section of the interval (compare, Figures 3 and 4), we suggest that the observed OCB in this local time sector may potentially be at higher latitudes than the Polar UVI instrument can detect.

[19] The model data comparison reported here goes well beyond the previous work [*Winglee et al.*, 1998; *Elsen et al.*, 1998; *Raeder et al.*, 1998, 2000; *Rae et al.*, 2004] in terms of validating global circulation models in two important aspects. First, using a unique 2-D OCB measurements, we are able to put much tighter constrains on the simulation results. Second, by comparing results of simulations with and without inner magnetosphere model we are able, for the first time, to identify its effects on the OCB location and pinpoint some of the deficiencies of the earlier modeling efforts.

[20] In the BATS-R-US and IE-only comparison, the maximum discrepancy between the model and our combined Polar UVI, SuperDARN, DMSP, and NOAA observations is ~10° around local dawn at the end of the simulated interval subsequent to substorm onset. Other discrepancies are more typically ~5° throughout the interval, and there are times where the observed and simulated OCBs are essentially colocated (see Figure 2). Although there are some marked differences between the real and simulated polar cap areas during this 2 h interval, there are similar trends in the modeled and observed OCB, which can be summarized as follows:

[21] 1. Following the southward turning, the polar cap area increases in both observations and the BATS-R-US-IE model, although this occurs faster in the model.

[22] 2. The model polar cap shrinks slightly after 1420 UT, indicating that the model is closing more flux than it is opening. This shrinkage occurs before the auroral brightening or substorm in the observational data set.

[23] The observed differences are perhaps not surprising as the BATS-R-US and IE-only model lacks a realistic inner magnetosphere, which is essential for accurate prediction of magnetotail dynamics [e.g., *Milan et al.*, 2009a]. Indeed, *Milan* [2009] demonstrated that both the coupling between the solar wind and the magnetosphere as well as the intensity of the ring current play vital roles in controlling the size of the auroral oval. Furthermore, because the ring current carries a large percentage of the total particle energy and sufficient current to directly affect the magnetic field configuration, this is obviously an important effect that is not addressed by all global circulation models (see review by *Toffoletto et al.* [2003]). Finally, there is also uncertainty in the role that numerical resistivity and viscosity plays in the MHD models.

[24] In the BATS-R-US, IE, and RCM coupled model, a more realistic description of the inner magnetosphere has been included, and the discrepancies between observed and modeled OCBs become significantly smaller as expected. Using this model configuration, the initial OCB can be described as much more circular, which leads to a better comparison of the observed and modeled OCBs during the northward IMF period (of the order of a few degrees separation at many local times and reproducing much of the dayside OCB excellently). In addition, the coupled model reproduces the dynamics of the OCB remarkably well subsequent to the southward IMF turning and prior to expansion phase onset. Interestingly, the modeled polar cap area is often identical (within experimental error) to the observed polar cap, even though there are some disagreements between the two boundaries in the dawn to midnight sector. One significant reason for this is that the underestimation of open flux in the midnight-dawn sector is balanced by the overestimation of open flux in the dusk sector. Note, however, that the dawn sector is the region where measuring the OCB location is most problematic. Importantly, the modeled polar cap area responds in the same manner as the observations, increasing as open flux is added to the dayside until the auroral brightening at ~1455 UT (though at a slightly faster rate) where the OCBs diverge at some local times, most notably in the dawn sectors, but are still accurate around the dusk sector, and reasonably accurate in the midnight and noon sectors. Overall, there is a good agreement between the observed and modeled OCBs during the ~90 min period surrounding the southward IMF turning and prior to expansion phase onset, where magnetotail dynamics clearly dominate the topology of the magnetosphere. Comparison between the simulation results with and without RCM model indicates that many of the imperfections in the OCB description in the past using MHD-based models can be attributed to the ring current effects. This is not surprising since the ring current has long been proposed to be a direct influence on the size of the auroral oval [e.g., *Feldstein and Starkov*, 1967; *Schultz*, 1997; *Yokoyama et al.*, 1998]. Until recently, however, global circulation models were unable to probe those effects directly, although a significant body of observational evidence points to such connection. For example, under geomagnetic storm conditions, part of the

inflation of the polar cap area can be attributed to IMF B_z, solar wind pressure, and storm time increases in geomagnetic tail field strength, but a significant other source can be the ring current itself [cf. *Feldstein*, 1969, p. 194]. Furthermore, *Stern* [1985] presented evidence that the ionospheric projection of the dayside cusp region can be displaced up to 2° equatorward for a *Dst* increase of ~100 nT. *Kalegaev et al.* [2001] found that under storm conditions, the magnetopause current, ring current, and tail current contributions to *Dst* were of the same order of magnitude and that the total energy of the ring current particles increases during periods of southward IMF. More recently, *Milan et al.* [2008, 2009a, 2009b] presented a statistical study on the influences on the radius of the auroral oval using the IMAGE spacecraft and a number of parameters internal and external to the magnetosphere. *Milan et al.* [2008, 2009a, 2009b] found that the radius of the auroral oval increases with enhancements in ring current intensity during geomagnetic storms. These authors hypothesize that the increase in polar cap area with ring current intensity is a function of both increased coupling at the dayside to inflate the polar cap area and a reduction of the tail reconnection rate such that the threshold for explosive energy release during a substorm is increased. Thus, the polar cap area is a function of both solar wind driving and ring current intensity. Furthermore, *Milan* [2009] went on to quantify the relationship of the size of the auroral oval and the solar wind-magnetosphere coupling together with the intensity of the ring current. *Milan* [2009] demonstrated that the coupling to the solar wind occurred on time scales of minutes to hours, whereas the quenching of magnetotail reconnection allowing the polar cap to inflate occurred on much longer time scales.

[25] In the model run without inner magnetospheric module, the polar cap area responds quicker, in agreement with *Milan et al.* [2009a, 2009b]. Including the ring current adds extra memory of the previous conditions and rigidity to the magnetospheric configuration. That is, in the absence of a ring current in the magnetosphere, the balance between dayside and nightside reconnection is achieved unrealistically quickly. In the model run including the RCM, the polar cap area inflates at the same rate as the observed polar cap area for ~2 h after a southward turning of the IMF and before substorm, again in agreement with *Milan et al.* [2009a, 2009b]. Under southward IMF conditions, the ring current exerts sufficient control over nightside reconnection processes to allow the polar cap area to inflate to a greater extent than it is possible in MHD-only models.

[26] In this paper we demonstrate that the inner magnetosphere plays a pivotal role in determining the size and shape of the auroral oval, a conclusion which has also been reached using observations [e.g., *Milan et al.*, 2008, 2009a, 2009b; *Milan*, 2009]. Future studies will investigate the relationship of polar cap flux and both observed and synthetic sym-H indices over a longer time period such as the 18 day period highlighted in the study of *Milan et al.* [2008].

5. Conclusions

[27] In this paper we presented two comparison runs of the SWMF model suite with an open-closed separatrix determination using combined Polar UVI, SuperDARN, DMSP, and NOAA observations for an interval including a northward to southward IMF transition. Time-dependent data from a variety of observational sources have been used and compared with the BATS-R-US-IE MHD model and the SWMF model including BATS-R-US, RCM, and IE modules.

[28] In the initial simulation without the Rice Convection Model, the best comparison between model and observation was found during the 30 min time interval between 1420 and 1450 UT, when the greatest discrepancy was no more than 5° of latitude. However, the rate of change of the OCB in the model is significantly faster than observations indicate. This can be attributed to one, or more sources: the lack of a real plasmasphere or ring current in that model configuration and greater reconnection rates within the model. To assess the importance of one of these parameters, we subsequently performed simulations of the OCB that incorporate effects of the ring current through the addition of the Rice Convection Model to the SWMF MHD model suite.

[29] With the inner magnetospheric physics of the RCM included, the observed and modeled OCBs were found to be consistent for almost 2 h following the southward turning of the IMF. In this subsequent comparison, the model responds in the same manner as the observed OCB to the southward turning of the IMF, and the OCB progresses to lower latitudes at all local times. We attribute both of these effects to the ring current which affects the nightside reconnection rate and allows the polar cap area to expand much further in the manner described by *Milan et al.* [2009a, 2009b]. Indeed, the calculated polar cap areas are identical within experimental error until substorm expansion phase onset occurs, which indicates that the same amount of magnetic energy is stored in the modeled magnetosphere as in the real magnetosphere. In our case study, we show that the observed and modeled OCBs are within ~degrees of each other at almost all magnetic local times, showing that the coupled BATS-R-US-IE-RCM models provide an accurate representation of the large-scale magnetospheric dynamics during this period. It is not until the data reveal an auroral brightening and following substorm that the observed and modeled OCBs diverge significantly. Because substorm dynamics are variable in nature and involve physics that is not captured in the global MHD models used in this study, this is not surprising.

[30] Our study presents a favorable time-dependent 2-D comparison of the open-closed field line boundary against near-global coverage data for a ~2 h period. The multidimensional nature of the observational data set used in comparison provides one of the most rigorous tests of first principle magnetospheric models to date and clearly illustrates the limitations of MHD-only approach. Our analysis is an important step toward the validation of global circulation models that are intended to reproduce magnetospheric dynamics in response to real-time solar wind conditions and clearly shows the important role of the inner magnetosphere in determining the boundaries between open and closed magnetic flux in the magnetosphere.

[31] **Acknowledgments.** The authors would like to thank CDAWeb and N.F. Ness for use of key parameter ACE spacecraft data and R. Lepping

and K. Ogilvie for the use of Wind Magnetic Fields Investigation and Solar Wind Experiment data, respectively. The authors thank G. Parks for providing Polar UVI data, and the PIs of the SuperDARN radars for provision of the radar data. This work was partially funded by both the Canadian Space Agency and the Natural Sciences and Engineering Research Council of Canada, including a Discovery Grant awarded to J.C. Samson. S.E.M. was supported by the Science and Technology Facilities Council (United Kingdom). Simulation results were obtained using the SWMF, developed by the Center for Space Environment Modeling, at the University of Michigan with funding support from NASA ESS, NASA ESTO-CT, NSF KDI, and DoD MURI. This research has been enabled by the use of computing resources provided by WestGrid and Compute/Calcul Canada.

[32] Masaki Fujimoto thanks the reviewers for their assistance in evaluating this paper.

References

Baker, J. B., C. R. Clauer, A. J. Ridley, V. O. Papitashvili, M. J. Brittnacher, and P. T. Newell (2000), The nightside poleward boundary of the auroral oval as seen by DMSP and the Ultraviolet Imager, *J. Geophys. Res.*, *105*(A9), doi:10.1029/1999JA000363.

Boakes, P. D., S. E. Milan, G. A. Abel, M. P. Freeman, G. Chisham, and B. Hubert (2009), A statistical study of the open magnetic flux content of the magnetosphere at the time of substorm onset, *Geophys. Res. Lett.*, *36*, L04105, doi:10.1029/2008GL037059.

Carbary, J. F., T. Sortirelis, P. T. Newell, and C.-I. Meng (2003), Auroral boundary correlations between UVI and DMSP, *J. Geophys. Res.*, *108*(A1), 1018, doi:10.1029/2002JA009378.

Cowley, S. W. H., and M. Lockwood (1992), Excitation and decay of solar wind-driven flows in the magnetosphere-ionosphere system, *Ann. Geophys.*, *10*, 103–115.

Chisham, G., and M. P. Freeman (2005), An investigation of high latitudinal transitions in the SuperDARN Doppler spectral width parameter at different magnetic local times, *Geophys. Res. Lett.*, *31*, L02804, doi:10.1029/2003GL019074.

Chisham, G., M. P. Freeman, T. Sotirelis, R. A. Greenwald, M. Lester, and J.-P. Villain (2005), A statistical comparison of SuperDARN spectral width boundaries and DMSP particle precipitation boundaries in the nightside ionosphere, *Ann. Geophys.*, *23*, 733–743.

De Zeeuw, D. L., S. Sazykin, R. A. Wolf, T. I. Gombosi, A. J. Ridley, and G. Toth (2004), Coupling of a global MHD code and an inner magnetospheric model: Initial results, *J. Geophys. Res.*, *109*, A12219, doi:10.1029/2003JA010366.

Elsen, R. K., R. M. Winglee, J. F. Spann, G. A. Germany, M. Brittnacher, and G. K. Parks (1998), The auroral oval boundaries on January 10, 1997: A comparison of global magnetospheric simulations with UVI images, *Geophys. Res. Lett.*, *25*, 2585–2588.

Evans, L. C., and E. C. Stone (1972), Electron polar cap and the boundary of open geomagnetic field lines, *J. Geophys. Res.*, *77*(28), 5580–5584, doi:10.1029/JA077i028p05580.

Fedder, J. A., and J. G. Lyon (1995), The Earth's magnetosphere is 165 R_E long: Self-consistent currents, convection, magnetospheric structure, and processes for northward interplanetary magnetic field, *J. Geophys. Res.*, *100*, 3623–3635.

Fedder, J. A., et al. (1997), A first comparison of POLAR magnetic field measurements and magnetohydrodynamic simulation results for field-aligned currents, *Geophys. Res. Lett.*, *24*, 2491–2494, doi:10.1029/97GL02608.

Feldstein, Y. I. (1969), Polar auroras, polar substorms, and their relationships with the dynamics of the magnetosphere, *Rev. Geophys.*, *7*, 179–218.

Feldstein, Y., and G. V. Starkov (1967), Dynamics of auroral belts and geomagnetic disturbances, *Planet. Space Sci.*, *15*, 209–229.

Garcia, K. S., and W. J. Hughes (2007), Finding the Lyon-Fedder-Mobarry magnetopause: A statistical perspective, *J. Geophys. Res.*, *112*, A06229, doi:10.1029/2006JA012039.

Gombosi, T. I., D. L. DeZeeuw, C. P. T. Groth, and K. G. Powell (2000), Magnetospheric configuration for Parker-spiral IMF conditions: results of a 3-D MHD simulation, *Adv. Space. Res.*, *26*, 139–149.

Greenwald, R. A., et al. (1995), DARN/SuperDARN: A global view of the dynamics of high-latitude convection, *Space Sci. Rev.*, *71*, 761–796.

Hubert, B., S. E. Milan, A. Grocott, C. Blockx, S. W. H. Cowley, and J.-C. Gérard (2006), Dayside and nightside reconnection rates inferred from IMAGE FUV and Super Dual Auroral Radar Network data, *J. Geophys. Res.*, *111*, A03217, doi:10.1029/2005JA011140.

Kabin, K., R. Rankin, R. Marchand, T. I. Gombosi, C. R. Clauer, A. J. Ridley, V. O. Papitashvili, and D. L. DeZeeuw (2003), Dynamic response of Earth's magnetosphere to B_y reversals, *J. Geophys. Res.*, *108*(A3), 1132, doi:10.1029/2002JA009480.

Kabin, K., R. Rankin, G. Rostoker, R. Marchand, I. J. Rae, A. J. Ridley, T. I. Gombosi, C. R. Clauer, and D. L. De Zeeuw (2004), Open-closed field line boundary position: A parametric study using an MHD model, *J. Geophys. Res.*, *109*, A05222, doi:10.1029/2003JA010168.

Kalegaev, V. V., I. I. Alexeev, and Ya. I. Feldstein (2001), The geotail and ring current dynamics under disturbed conditions, *J. Atmos. Sol.-Terr. Phys.*, *63*, 473–479, doi:10.1016/S1364-6826(00)00162-0.

Kauristie, K., J. Weygand, T. I. Pulkkinen, J. S. Murphree, and P. T. Newell (1999), Size of the auroral oval: UV ovals and precipitation boundaries compared, *J. Geophys. Res.*, *104*(A2), doi:10.1029/1998JA900046.

McFadden, J. P., C. W. Carlson, D. Larson, J. Bonnell, F. Mozer, V. Angelopoulos, K.-H. Glassmeier, and U. Auster (2008), THEMIS ESA first science results and performance issues, *Space Sci. Rev.*, *141*, 477–508, doi:10.1007/s11214-008-9433-1.

Milan, S. E. (2009), Both solar wind-magnetosphere coupling and ring current intensity control of the size of the auroral oval, *Geophys. Res. Lett.*, *36*, L18101, doi:10.1029/2009GL039997.

Milan, S. E., M. Lester, S. W. H. Cowley, K. Oksavik, M. Brittnacher, R. A. Greenwald, G. Sofko, and J.-P. Vilain (2003), Variations in polar cap area during two substorm cycles, *Ann. Geophys.*, *21*(5), 1121–1140.

Milan, S. E., G. Provan, and B. Hubert (2007), Magnetic flux transport in the Dungey cycle: A survey of dayside and nightside reconnection rates, *J. Geophys. Res.*, *112*, A01209, doi:10.1029/2006JA011642.

Milan, S. E., P. D. Boakes, and B. Hubert (2008), Response of the expanding/contracting polar cap to weak and strong solar wind driving: Implications for substorm onset, *J. Geophys. Res.*, *113*, A09215, doi:10.1029/2008JA013340.

Milan, S. E., J. Hutchinson, P. D. Boakes, and B. Hubert (2009a), Influences on the radius of the auroral oval, *Ann. Geophys.*, *27*, 2925–2936.

Milan, S. E., A. Grocott, C. Forsyth, S. M. Imber, P. D. Boakes, and B. Hubert (2009b), A superposed epoch analysis of auroral evolution during substorm growth, onset and recovery: Open magnetic flux control of substorm intensity, *Ann. Geophys.*, *27*, 659–668.

Ogino, T. (1986), A three-dimensional MHD simulation of the interaction of the solar wind with the Earth's magnetosphere: The generation of field-aligned currents, *J. Geophys. Res.*, *91*, 6791–6806.

Powell, K. G., P. L. Roe, T. J. Linde, T. I. Gombosi, and D. L. DeZeeuw (1999), A solution-adaptive upwind scheme for ideal magnetohydrodynamics, *J. Comput. Phys.*, *154*, 284–309.

Rae, I. J., K. Kabin, R. Rankin, F. R. Fenrich, W. Liu, J. A. Wanliss, A. J. Ridley, T. I. Gombosi, and D. L. De Zeeuw (2004), Comparison of photometer and global MHD determination of the open-closed field line boundary, *J. Geophys. Res.*, *109*, A01204, doi:10.1029/2003JA009968.

Raeder, J., R. J. Walker, and M. Ashourabdalla (1995), The structure of the distant geomagnetic tail during long periods of northward IMF, *Geophys. Res. Lett.*, *22*, 349–352.

Raeder, J., J. Berchem, and M. Ashour-Abdalla (1998), The Geospace Environment Modeling Grand Challenge: Results from a global circulation model, *J. Geophys. Res.*, *103*, 14,787–14,797.

Raeder, J., R. L. McPherron, L. A. Frank, S. Kokubun, G. Lu, T. Mukai, W. R. Paterson, J. B. Sigwarth, H. J. Singer, and J. A. Slavin (2000), Global simulation of the Geospace Environment Modeling substorm challenge event, *J. Geophys. Res.*, *106*, 381–395.

Ridley, A. J., K. C. Hansen, G. Toth, D. L. De Zeeuw, T. I. Gombosi, and K. G. Powell (2002), University of Michigan MHD results of the geospace global circulation model metrics challenge, *J. Geophys. Res.*, *107*(A10), 1290, doi:10.1029/2001JA000253.

Schultz, M. (1997), Direct influence of ring current on auroral oval diameter, *J. Geophys. Res.*, *102*, 14,149–14,154.

Song, P., D. L. DeZeeuw, T. I. Gombosi, C. P. T. Groth, and K. G. Powell (1999), A numerical study of solar wind-magnetosphere interaction for northward interplanetary magnetic field, *J. Geophys. Res.*, *104*, 28,361–28,378, doi:10.1029/1999JA900378.

Stern, D. P. (1985), Parabolic harmonics in magnetospheric modeling: The main dipole and the ring current, *J. Geophys. Res.*, *90*, 10,851–10,863.

Su, Y.-J., J. E. Borovsky, M. F. Thomsen, R. C. Elphic, and D. J. McComas (2000), Plasmapheric material at the reconnecting magnetopause, *J. Geophys. Res.*, *105*(A4), 7591–7600, doi:10.1029/1999JA000266.

Toffoletto, F., S. Sazykin, R. Spiro, and R. Wolf (2003), Inner magnetospheric modeling with the Rice Convection Model, *Space Sci. Rev.*, *107*(1–2), 175–196.

Torr, M. R., et al. (1995), A far ultraviolet imager for the International Solar-Terrestrial Physics Mission, *Space Sci. Rev.*, *71*, 329–383.

Toth, G., et al. (2005), Space Weather Modeling Framework: A new tool for the space science community, *J. Geophys. Res.*, *110*, A12226, doi:10.1029/2005JA011126.

Toth, G., D. L. De Zeeuw, T. I. Gombosi, W. B. Manchester, A. J. Ridley, I. V. Sokolov, and I. I. Roussev (2007), Sun-to-thermosphere simulation

of the 28–30 October 2003 storm with the Space Weather Modeling Framework, *Space Weather*, *5*, S06003, doi:10.1029/2006SW000272.

Tsyganenko, N. A. (1996), Effects of the solar wind conditions on the global magnetospheric configuration as deduced from data-based models, in Proceedings of ICS-3 Conference on Substorms, Versailles, France, Eur. Space Agency Spec. Publ., ESA SP-389, 181.

Watanabe, M., K. Kabin, G. J. Sofko, R. Rankin, T. I. Gombosi, A. J. Ridley, and C. R. Clauer (2005), Internal reconnection for northward interplanetary magnetic field, *J. Geophys. Res.*, *110*, A06210, doi:10.1029/2004JA010832.

White, W. W., G. L. Siscoe, G. M. Erickson, Z. Kaymaz, N. C. Maynard, K. D. Siebert, B. U. O. Sonnerup, and D. R. Weimer (1998), The magnetospheric sash and the cross-tail S, *Geophys. Res. Lett.*, *25*, 1605–1608.

Wild, J. A., S. E. Milan, C. J. Owen, J. M. Bosqued, M. Lester, D. M. Wright, H. Frey, C. W. Carlson, A. N. Fazakerley, and H. Reme (2004), The location of the open-closed magnetic field line boundary in the dawn sector auroral ionosphere, *Ann. Geophys.*, *22*, 3625–3639.

Winglee, R. M., S. Kokubun, R. P. Lin, and R. P. Lepping (1998), Flux rope structures in the magnetotail: Comparison between Wind/Geotail observations and global simulations, *J. Geophys. Res.*, *103*, 135–150, doi:10.1029/97JA02415.

Yahnin, A., et al. (1994), Features of steady magnetospheric convection, *J. Geophys. Res.*, *99*, 4039–4051.

Yokoyama, N., Y. Kamide, and H. Miyaoka (1998), The size of the auroral belt during magnetic storms, *Ann. Geophys.*, *16*, 566–573.

Zhang, J., et al. (2007), Understanding storm-time ring current development through data-model comparisons of a moderate storm, *J. Geophys. Res.*, *112*, A04208, doi:10.1029/2006JA011846.

C. R. Clauer, Department of Electrical and Computer Engineering, 302 Whittemore Hall, Virginia Polytechnic Institute and State University, Blacksburg, VA 24061-0111, USA.

D. L. DeZeeuw, T. I. Gombosi, A. J. Ridley, and G. Tóth, Center for Space Environment Modeling, University of Michigan, Ann Arbor, MI 48109, USA.

F. R. Fenrich, K. Kabin, I. J. Rae, R. Rankin, and C. E. J. Watt, Department of Physics, University of Alberta, Edmonton, AB T6G 2J1, Canada. (jonathan.rae@ualberta.ca)

J. Y. Lu, National Center for Space Weather, China Meteorology Administration, Beijing 100081, China.

S. E. Milan, Department of Physics and Astronomy, University of Leicester, Leicester LE1 7RH, UK.

J.-C. Zhang, Space Science Center, University of New Hampshire, Durham, NH 03824, USA.